RESEARCH ARTICLE

Harmonic Solution of Higher-Dimensional Second Order Kuramoto Oscillator Network

JING LI[ID], **ZHENYAO LI**[ID], **DEQIANG GAN**[ID], **(Senior Member, IEEE), AND HAO WU**[ID], **(Senior Member, IEEE)**

College of Electrical Engineering, Zhejiang University, Hangzhou 310027, China

Corresponding author: Deqiang Gan (dgan@zju.edu.cn)

ABSTRACT Obtaining the solution of Kuramoto oscillator model is an effective way to understand the mechanism behind the dynamical behaviors it represents. However, it is not an easy work to get, even the approximation solution for the second order Kuramoto oscillator network because of its complex coupling interaction and strong nonlinearity. Hence, this paper first establishes a new polynomial mathematical model for the second order Kuramoto oscillator network, which is partly decoupled in a polynomial fashion. Then, a quadratic harmonic balance method (HBM) is developed to get the approximate solution for quadratic differential algebraic equation (QDAE) system. An equivalent quadratic technique is introduced to convert the polynomial Kuramoto oscillator model into a QDAE system aiming to obtain its harmonic solution. Finally, the suggested harmonic solution is utilized to explain the morphological characteristics of the stable motion of oscillators, and the relative motions for the oscillators in Kuramoto network is concluded by a set of nonlinear state output equations. It is also found that the distance between the maximum phase angle and the controlling unstable equilibrium point (UEP) can be used as a stability margin for the oscillator network. A single-machine infinite bus (SMIB) power system, an IEEE 3-machine 9-bus power system and an IEEE 10-machine 39-bus power system are employed as different dimension second order Kuramoto oscillator network cases to demonstrate the validation and accuracy of the proposed method and analysis.

INDEX TERMS Harmonic solution, HBM, Kuramoto oscillator network, QDAE, transient stability.

I. INTRODUCTION

The Kuramoto model has been introduced in 1975 to describe the motion of coupled particles [1]. In the last forty years, the second order Kuramoto oscillator model has been extended to study problems originated from many disciplines [2], [3], representing the dynamics of electron oscillators [4] in electric engineering, Josephson junction [5] and pendulum equation [6] in physics, synchronous machines [7] in power system community, and so forth. Different from the classical first order Kuramoto oscillator model, the second order Kuramoto model exhibits much more complicated behaviors because of the way of its complicated coupling interaction, posing a challenge for developing method to study the dynamical characteristic of this system it represents.

The associate editor coordinating the review of this manuscript and approving it for publication was Yifan Zhou.

As is well-known, it is very difficult to find closed-form solutions for second order Kuramoto models [8], [9], [10], [11]. Hence, it is natural to seek the approximate solution in order to understand the dynamic behavior of the second order Kuramoto oscillator network. In history, several attempts have been reported to get the analytical characteristic of the second order Kuramoto oscillator network. Some early results using asymptotic expansion methods were introduced in [12], [13], and [14] to approximate the stable manifolds of the UEP. Some approximate formulas were introduced in [15], [16], and [17] to represent stability region boundaries which are essentially composed of stable manifold of unstable equilibrium point (UEP) of the second order Kuramoto oscillator model. However, due to the inherent nonlinearity of second order Kuramoto oscillator network, the standard perturbation methods such as normal form method [13], [14], Krylov-Bogoli-Mitropolsky

method [18], Lindstedt-Poincaré method [19], multi-time scales method [20], do not perform satisfactorily. The results mentioned above focus on the behavior in the neighborhood of an UEP. Little attention has been paid to the behavior of Kuramoto oscillators inside the stability region of a stable equilibrium point (SEP). Furthermore, it has been recognized that the swing behavior of pendulum systems is typically quasi-periodical [21]. This indicates that the second order Kuramoto dynamic system has a natural low-pass filtering characteristic, revealing the potential of harmonic balance method (HBM) in studying the motion of Kuramoto oscillators.

Recently, the incremental HBM has been applied to estimate the limit cycle of swing equation in power system community [22], predicting the homoclinic bifurcation curve effectively, showing the potential of the HBM in dealing with strongly nonlinear systems. In the community of mechanical engineering, a numerical approach to obtain the quasi-periodic vibrations by HBM is developed in [23], demonstrating the satisfactory performance of HBM when the models are experiencing nonlinearities induced by strong engine order excitations. The periodic response of the systems subjected to harmonic forces is obtained by employing HMB method in [24], revealing the dynamic characteristic and vibration transmission behavior of oscillators system. HBM and Galerkin methods are used together to cam-follower system to estimate the steady-state response [25], which can predict the fundamental and sub-harmonic solutions accurately and efficiently. These results show the application potential of HBM in dealing with different nonlinear system, and have been extensively studied in various field. For more detailed technique and progress of HBM, the readers are referred to reference [26], [27], and [28], respectively.

Different from previous works focusing the analytical characteristic around the UEP of Kuramoto model mentioned before, this paper investigates the harmonic solution of higher-dimensional second order Kuramoto oscillator model within stability region of a SEP. In other words, the system trajectories reside inside stability region of a SEP. Firstly, a new polynomial model of Kuramoto oscillators network is established via Taylor expansion formula. Then, a multi-frequency quadratic harmonic balance method (QHBM) inspired by the result in [29] and [30], is developed. The method can find the harmonic solution by providing only some coefficient matrices related to the quadratic differential algebraic equation (QDAE) system. Thereby, based on the suggested harmonic solution, the relationships between the eigenvalues and dynamics of the Kuramoto oscillator model are examined, the relative motion equation system between different oscillators is established, and a new phase-domain stability margin index for higher-dimensional oscillator network is proposed based on the celebrated stability region theory. Finally, some power systems data are employed to show the effectiveness of the proposed method.

To sum up, the original contributions of this paper are threefold:

1) Model. A partly decoupled polynomial equation system for the second order Kuramoto model is derived in detail, revealing the morphological characteristics of stable motion of oscillators.

2) Methodology. A new QHBM based on QDAE system is developed systematically to obtain the steady-state or periodic response for zero-damping systems.

3) Analysis. The analysis of solution structure, relative motion of oscillators and large disturbance stability is presented based the obtained harmonic solution.

The rest of the paper is organized as follows. In Section II, a new polynomial model for the second order Kuramoto oscillator network is established, and the structural properties of the derived polynomial equations are presented. Section III gives the fundamental basis of the QHBM rigorously, which provide the details of forming harmonic algebraic equation (HAE). In Section IV, an equivalent quadratic conversion technique is introduced to obtain the harmonic solution of second order Kuramoto oscillator network. Section V investigates the analytical characteristic of second order Kuramoto oscillator network based on the harmonic solution. Section VI shows the effectiveness of the proposed method and analysis using several power system test cases as examples. Section VII concludes this paper.

II. A NEW POLYNOMIAL MODEL FOR SECOND-ORDER KURAMOTO OSCILLATOR NETWORK

In this section, a polynomial model for second order Kuramoto oscillator network is derived firstly. The model is formulated in matrix form so it can accommodate Kuramoto model with arbitrary number of oscillators. An eigen transformation is introduced later to decouple the polynomial model into two subsystems.

A. A TAYLOR EXPANSION FORMULATION FOR SECOND ORDER KURAMOTO NETWORK WITH ANY NUMBER OF OSCILLATORS

Consider the second order Kuramoto oscillator network on a graph $\mathcal{G} \triangleq (N, \mathcal{E})$ as follows,

$$M_i\ddot{\delta}_i + D_i\dot{\delta}_i = \Omega_i - \sum_{j=1}^{n+1} a_{ij}\sin(\delta_i - \delta_j + \gamma_{ij}); \ i \in N, \quad (1)$$

where $N = \{1, 2, 3, \ldots, n, n+1\}$ and $\mathcal{E} = N \otimes N$ are the node set and edge set of $\mathcal{G}$, respectively. The symbol $\otimes$ represents Cartesian product. Here δ_i is the phase angle of oscillator i. a_{ij} is the stiffness of elastic spring between oscillator i and oscillator j. γ_{ij} is the phase shift between oscillator i and oscillator j. M_i and D_i are the inertial time constant and damping coefficient of oscillator i,respectively. Ω_i is the driving force of oscillator i. From physical perspective, the second order Kuramoto network is shown in FIGURE 1.
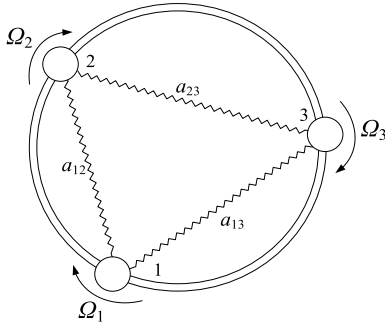
FIGURE 1. Illustration of the Kuramoto oscillator network.

The Taylor expansion formula is used to approximate the sine functions in the right-hand side (RHS) of (1) as follows,

$$\sin(\underbrace{\delta_i - \delta_j}_{\delta_{ij}} - \gamma_{ij})$$

$$= \delta_{ij} - \gamma_{ij} + \epsilon_3(\delta_{ij} - \gamma_{ij})^3$$
$$+ \epsilon_5(\delta_{ij} - \gamma_{ij})^5 + \epsilon_7(\delta_{ij} - \gamma_{ij})^7 + o\left((\delta_{ij} - \gamma_{ij})^7\right), \quad (2)$$

where $\epsilon_3 = -1/6, \epsilon_5 = 1/120, \epsilon_7 = -1/5040$. Furthermore, the equilibrium point is moving to the origin by introducing coordinate transformation $\boldsymbol{y} = \boldsymbol{\delta} - \bar{\boldsymbol{\delta}}$, here $\bar{\boldsymbol{\delta}}$ indicates a SEP of (1). Substituting the (2) into (1), the RHS of (1) can be written as follows,

RHS

$$= \Omega_i - \sum_{j=1}^{n+1} a_{ij} \begin{bmatrix} \delta_{ij} - \gamma_{ij} + \epsilon_3(\delta_{ij} - \gamma_{ij})^3 \\ + \epsilon_5(\delta_{ij} - \gamma_{ij})^5 + \epsilon_7(\delta_{ij} - \gamma_{ij})^7 \end{bmatrix}$$

$$= \Omega_i - \sum_{j=1}^{n+1} a_{ij} \begin{bmatrix} y_{ij} + \underbrace{\bar{\delta}_{ij} - \gamma_{ij}}_{\varsigma_{ij}} + \epsilon_3(y_{ij} + \underbrace{\bar{\delta}_{ij} - \gamma_{ij}}_{\varsigma_{ij}})^3 \\ + \epsilon_5(y_{ij} + \underbrace{\bar{\delta}_{ij} - \gamma_{ij}}_{\varsigma_{ij}})^5 + \epsilon_7(y_{ij} + \underbrace{\bar{\delta}_{ij} - \gamma_{ij}}_{\varsigma_{ij}})^7 \end{bmatrix}$$

$$= \underbrace{\Omega_i - \sum_{j=1}^{n+1} a_{ij}(\varsigma_{ij} + \epsilon_3 \varsigma_{ij}^3 + \epsilon_7 \varsigma_{ij}^7 + \epsilon_7 \varsigma_{ij}^7)}_{=0}$$

$$- \sum_{j=1}^{n+1} \left(a_{1,ij} y_{ij} + a_{2,ij} y_{ij}^2 + a_{3,ij} y_{ij}^3\right)$$

$$- \sum_{j=1}^{n+1} \left(a_{4,ij} y_{ij}^4 + a_{5,ij} y_{ij}^5 + a_{6,ij} y_{ij}^6 + a_{7,ij} y_{ij}^7\right). \quad (3)$$

Plugging (3) into (1), the polynomial Kuramoto model in $\boldsymbol{y}$ coordinate system is obtained as follows,

$$M_i \ddot{y}_i + D_i \dot{\delta}_i$$

$$= - \sum_{j=1}^{n+1} \left(a_{1,ij} y_{ij} + a_{2,ij} y_{ij}^2 + a_{3,ij} y_{ij}^3\right)$$

$$- \sum_{j=1}^{n+1} \left(a_{4,ij} y_{ij}^4 + a_{5,ij} y_{ij}^5 + a_{6,ij} y_{ij}^6 + a_{7,ij} y_{ij}^7\right), \quad (4)$$

where coefficients in (4) are shown as follows,

$$\begin{cases} a_{1,ij} = a_{ij}\left(1 + 3\epsilon_3 \zeta_{ij}^2 + 5\epsilon_5 \zeta_{ij}^4 + 7\epsilon_7 \zeta_{ij}^6\right) \\ a_{2,ij} = a_{ij}\left(3\epsilon_3 \zeta_{ij} + 10\epsilon_5 \zeta_{ij}^3 + 21\epsilon_7 \zeta_{ij}^5\right) \\ a_{3,ij} = a_{ij}\left(\epsilon_3 + 10\epsilon_5 \zeta_{ij}^2 + 35\epsilon_7 \zeta_{ij}^4\right) \\ a_{4,ij} = a_{ij}\left(5\epsilon_5 \zeta_{ij} + 35\epsilon_7 \zeta_{ij}^3\right) \\ a_{5,ij} = a_{ij}\left(\epsilon_5 + 21\epsilon_7 \zeta_{ij}^2\right) \\ a_{6,ij} = a_{ij}\left(7\epsilon_7 \zeta_{ij}\right) \\ a_{7,ij} = a_{ij}\epsilon_7. \end{cases} \quad (5)$$

In order to write RHS of (4) into matrix form, the following coefficient matrix $\boldsymbol{P}$ is defined as follows,

$$\boldsymbol{Py} = \left[y_{12}, \cdots, y_{1,n+1}, y_{23}, \cdots, y_{ij}, \cdots, y_{2,n+1}, \cdots, y_{n,n+1}\right]^T, \quad (6)$$

where $y_{ij} = y_i - y_j, 1 \le i < j \le n+1$ is the angle difference in $\boldsymbol{y}$ coordinate system. Hence, the matrix form of (4) can be represented as follows,

$$\boldsymbol{My''} + \boldsymbol{Dy'} = -\boldsymbol{A}_1 \boldsymbol{y} + \sum_{k=2}^{7} \boldsymbol{A}_k \left[diag\left(\boldsymbol{Py}\right)\right]^{k-1} \boldsymbol{Py}, \quad (7)$$

where $\boldsymbol{M} = diag(M_1, \cdots, M_n)$ and $\boldsymbol{D} = diag(D_1, \cdots, D_n)$ are the inertial and damping matrix, respectively. The coefficient matrixes $\boldsymbol{A}_{\{2,3,\cdots,7\}} \in \mathbb{R}^{(n+1)\times[(n+1)n/2]}$ are corresponding to (4), separately. Specifically, $\boldsymbol{A}_1$ can be written as follows,

$$\boldsymbol{A}_1 = \begin{cases} \sum_{j=1,j\neq i}^{n+1} a_{1,ij} & i = j \\ -a_{1,ij} & i \neq j, \end{cases} \quad (8)$$

where $\boldsymbol{A}_1 \in \mathbb{R}^{(n+1)\times(n+1)}$ is the Laplacian matrix of graph $\mathcal{G}$ Therefore, $\boldsymbol{A}_1$ can be formulated via algebraic graph operation equivalently, i.e., $\boldsymbol{A}_1 = diag(\boldsymbol{A}\mathbf{1}_n) - \boldsymbol{A}$, where $\boldsymbol{A} = (a_{1,ij}) \in \mathbb{R}^{(n+1)\times(n+1)}$ is the adjacency matrices of graph $\mathcal{G}$, and $\mathbf{1}_n$ is vector with 1 being the entries with appropriate dimension.

Notice that the matrix $\boldsymbol{P}$ has structural characteristic because of the constraint imposed by (6). Without loss of generality, an example with $n = 3$ is illustrated as follows,

$$\begin{bmatrix} y_1 - y_2 \\ y_1 - y_3 \\ y_1 - y_4 \\ y_2 - y_3 \\ y_2 - y_4 \\ y_3 - y_4 \end{bmatrix} = \underbrace{\begin{bmatrix} 1 & -1 & 0 & 0 \\ 1 & 0 & -1 & 0 \\ 1 & 0 & 0 & -1 \\ 0 & 1 & -1 & 0 \\ 0 & 1 & 0 & -1 \\ 0 & 0 & 1 & -1 \end{bmatrix}}_{\boldsymbol{P}} \begin{bmatrix} y_1 \\ y_1 \\ y_3 \\ y_4 \end{bmatrix}. \quad (9)$$

It can be seen that $\boldsymbol{P} \cdot \mathbf{1} = \mathbf{0}$ from (9), which means that the summation of any row of $\boldsymbol{P}$ is equal to 0. Denoting the symbol $\mathcal{L}$ indicating the set of zero row sum matrix, then we have $\boldsymbol{P}, \boldsymbol{A}_1 \in \mathcal{L}$.

B. AN EIGEN TRANSFORMATION TO POLYNOMIAL KURAMOTO MODEL

An eigen transformation $y = \mathcal{U}z$ is introduced as follows,

$$\begin{cases} M^{-1} \cdot A_1 = \mathcal{U} \cdot \Lambda^2 \cdot \mathcal{U}^{-1} \\ \Lambda^2 = diag(\lambda_1^2, \cdots, \lambda_n^2, 0) \\ \mathcal{U} = [u_1, \cdots, u_n, 1] = [u, 1], \end{cases} \quad (10)$$

where $\lambda_1^2 \leq \lambda_2^2 \leq \cdots \leq \lambda_n^2$ are the n nonzero eigenvalues of the matrix $M^{-1}A_1$ because of its zero-row sum property. Considering $P \in \mathcal{L}$, one obtains,

$$P \in \mathcal{L} \quad \Rightarrow \quad P \cdot \mathcal{U} = P \cdot [u, 1] = [\alpha, 0], \quad (11)$$

where $\alpha \in \mathbb{R}^{n_\alpha \times n}$, $n_\alpha = (n+1)n/2$. Plugging transformation $y = \mathcal{U}z$ into (7) with the aid of (10) and (11), a partly decoupled polynomial model is obtained as follows,

$$\begin{bmatrix} z''_1 \\ z''_{n+1} \end{bmatrix} + \mathcal{U}^{-1}M^{-1}D\mathcal{U} \begin{bmatrix} z'_1 \\ z'_{n+1} \end{bmatrix}$$
$$= -\begin{bmatrix} \lambda^2 \\ & 0 \end{bmatrix} \begin{bmatrix} z_1 \\ z_{n+1} \end{bmatrix}$$
$$+ \begin{bmatrix} \sigma_1 \\ \sigma_2 \end{bmatrix} \sum_{k=2}^{7} \Big(A_k [diag(\alpha z_1)]^{k-1} \alpha z_1 \Big), \quad (12)$$

where $z = [z_1, z_{n+1}]$, $\lambda^2 = diag(\lambda_1^2, \cdots, \lambda_n^2)$, $\sigma = \mathcal{U}^{-1}M^{-1}$, and $\sigma^T = [\sigma_1^T, \sigma_2^T]$. Suppose that there is uniform damping in Kuramoto network [31], i.e., $D_i/M_i = \mu$, then (12) can be written as follows,

$$\begin{cases} z''_1 + \mu z'_1 = -\lambda^2 z_1 \\ \quad + \sum_{k=2}^{7} \Big(\sigma_1 A_k [diag(\alpha z_1)]^{k-1} \alpha z_1 \Big) \\ \quad = -\lambda^2 z_1 + g_{nl}(z_1) \quad (I) \\ z''_{n+1} + \mu z'_{n+1} = \sum_{k=2}^{7} \Big(\sigma_2 A_k [diag(\alpha z_1)]^{k-1} \alpha z_1 \Big) \\ \quad = f_{nl}(z_1) \quad (II), \end{cases} \quad (13)$$

where $g_{nl} : \mathbb{R}^n \to \mathbb{R}^n, f_{nl} : \mathbb{R}^n \to \mathbb{R}$ are all polynomial functions. It can be observed that (13)-(I) is completely decoupled from variable z_{n+1}, and (13)-(II) completely depends on the main subsystem variable z_1, revealing the partly decoupled characteristic.

III. A QUADRATIC HARMONIC BALANCE METHOD

In this section, a QHBM for QDAE systems is developed systematically. The principle of QHBM is reviewed in Section III-A, and the detailed procedure on how forming HAE of QDAE system to obtain harmonic solution is presented from Section III-B to III-D.

A. THE PRINCIPLE OF QHBM [29], [30]

Consider the following initial value problem of QDAE system,

$$m(\dot{X}) = c + l(X) + q(X, X)$$

$$X(0) = X_{ini0}, \quad (14)$$

where $X \in \mathbb{R}^{n_e}$ is unknowns. $m : \mathbb{R}^{n_e} \to \mathbb{R}^{n_e}$ is a linear vector function acting on the derivative of X. $l : \mathbb{R}^{n_e} \to \mathbb{R}^{n_e}$ and $q : \mathbb{R}^{n_e} \times \mathbb{R}^{n_e} \to \mathbb{R}^{n_e}$ are linear vector function and quadratic bilinear function acting on X, respectively.

Suppose that the system (14) has a periodic solution with prior knowledge, and the form of this periodic solution is assumed as follows,

$$X(t) = a + \sum_{k=1}^{H} b_k \cos k\omega t + \sum_{k=1}^{H} c_k \sin k\omega t$$
$$= \underbrace{a}_{x_0} + \sum_{k=1}^{H} \underbrace{(b_k \cos k\omega t + c_k \sin k\omega t)}_{x_k} = \sum_{k=0}^{H} x_k, \quad (15)$$

where $a \in \mathbb{R}^{n_e \times 1}$ is a constant term, and $b_k, c_k \in \mathbb{R}^{n_e \times n_e}$ are the harmonic coefficients, and $\omega^T = [\omega_1, \omega_2, \ldots, \omega_{n_e}]^T$ is the frequency vector of harmonic solution, and the symbol H is the maximum order of harmonic. Denote the unknown vector appeared in (15) as follows,

$$U^T = \begin{bmatrix} a^T, row(b_1)^T, row(c_1)^T, \cdots \\ \cdots, row(b_H)^T, row(c_H)^T \end{bmatrix}, \quad (16)$$

where the symbol $row(b)$ indicates the column vector sorted by row vector of matrix b consecutively, and the unknown variable is $U \in \mathbb{R}^{(n_e \times n_e) \times 2H + n_e}$.

Inserting the period solution (15) into (14), each harmonic is collected consecutively according to ascending order of harmonics. After some manipulations, it is not difficult to observe that the unknown vector satisfies $n_e \times n_e \times 2H + n_e$ HAE as follows,

$$M(U) = C + L(U) + Q(U, U), \quad (17)$$

where symbols $M(\cdot), C, L(\cdot), Q(\cdot, \cdot)$ are all operators acting on the variable U, which only depends on the details of the QDAE system (14) and harmonic order H.

Adding equations generated by the initial value in (14), one obtains n_e equations as follows,

$$X(0) = a + \sum_{k=1}^{H} (b_k \cdot 1) = X_{ini0}. \quad (18)$$

It can be observed that the dimension of $[U^T, \omega^T]$ is equal to $2H \times n_e^2 + 2n_e$, which is same with the number of equations simultaneous (17) and (18). Hence, some standard iterative method can be used to solve the algebra equations.

B. LINEAR OPERATOR M(·), L(·) AND CONSTANT OPERATOR C

The linear operator $m(\cdot)$ in (14) can be written as follows,

$$m(\dot{X}(t)) = \mathbb{D}\dot{X}(t), \quad (19)$$

where $\mathbb{D} \in \mathbb{R}^{n_e \times n_e}$ is a specific constant matrix depending on the detail of operator $m(\cdot)$ in (14). Specifically, (19) can be

formulated as follows,

$$
\mathbb{D}\dot{\boldsymbol{X}}(t) = \mathbb{D}\left(\boldsymbol{a} + \sum_{k=1}^{H} \boldsymbol{b}_k \cos k\boldsymbol{\omega}t + \sum_{k=1}^{H} \boldsymbol{c}_k \sin k\boldsymbol{\omega}t\right)'
$$

$$
= \sum_{k=1}^{H} \underbrace{k\mathbb{D}\boldsymbol{c}_k diag(\boldsymbol{\omega})}_{\boldsymbol{Y}_{c,k}} \cos(k\boldsymbol{\omega}t)
$$

$$
- \sum_{k=1}^{H} \underbrace{k\mathbb{D}\boldsymbol{b}_k diag(\boldsymbol{\omega})}_{-\boldsymbol{Y}_{s,k}} \sin(k\boldsymbol{\omega}t)
$$

$$
= \sum_{k=1}^{H} \boldsymbol{Y}_{c,k} \cos(k\boldsymbol{\omega}t) + \sum_{k=1}^{H} \boldsymbol{Y}_{s,k} \sin(k\boldsymbol{\omega}t). \quad (20)
$$

Hence, $\boldsymbol{M}(\boldsymbol{U})$ in (17) can be formulated according to the order of harmonic as follows,

$$
\boldsymbol{M}(\boldsymbol{U}) = \left[\boldsymbol{0}^T, \mathbf{row}(\boldsymbol{Y}_{c,1})^T, \mathbf{row}(\boldsymbol{Y}_{s,1})^T, \cdots \\ \cdots, \mathbf{row}(\boldsymbol{Y}_{c,H})^T, \mathbf{row}(\boldsymbol{Y}_{s,H})^T\right]^T,
$$

$$(21)$$

where $\boldsymbol{M}(\boldsymbol{U}) \in \mathbb{R}^{(n_e \times n_e) \times 2H + n_e}$.

The constant operator $\boldsymbol{C}$ in (17) is the zeros order harmonic corresponding to the constant term in (14). Hence, we have,

$$
\boldsymbol{C} = \left[\boldsymbol{c}^T, \boldsymbol{0}^T, \boldsymbol{0}^T, \ldots, \boldsymbol{0}^T\right]^T, \quad (22)
$$

where $\boldsymbol{C} \in \mathbb{R}^{(n_e \times n_e) \times 2H + n_e}$.

The linear operator $\boldsymbol{l}(\cdot)$ in (14) can be written into matrix form as follows,

$$
\boldsymbol{l}(\boldsymbol{X}) = \mathbb{L}\boldsymbol{X} = \mathbb{L}\left[\boldsymbol{a} + \sum_{k=1}^{H} \boldsymbol{b}_k \cos k\boldsymbol{\omega}t + \sum_{k=1}^{H} \boldsymbol{c}_k \sin k\boldsymbol{\omega}t\right]
$$

$$
= \mathbb{L}\boldsymbol{a} + \sum_{k=1}^{H} \mathbb{L}\boldsymbol{b}_k \cos(k\boldsymbol{\omega}t) + \sum_{k=1}^{H} \mathbb{L}\boldsymbol{c}_k \sin(k\boldsymbol{\omega}t), \quad (23)
$$

where $\mathbb{L} \in \mathbb{R}^{n_e \times n_e}$ is a specific constant matrix corresponding to the detail of operator $\boldsymbol{l}(\cdot)$ in (14). Thus, $\boldsymbol{L}(\boldsymbol{U})$ in (17) can be obtained as follows,

$$
\boldsymbol{L}(\boldsymbol{U}) = \left[(\mathbb{L}\boldsymbol{a})^T, \mathbf{row}(\mathbb{L}\boldsymbol{b}_1)^T, \mathbf{row}(\mathbb{L}\boldsymbol{c}_1)^T, \cdots \\ \cdots, \mathbf{row}(\mathbb{L}\boldsymbol{b}_H)^T, \mathbf{row}(\mathbb{L}\boldsymbol{c}_H)^T\right]^T,
$$

$$(24)$$

where $\boldsymbol{L}(\boldsymbol{U}) \in \mathbb{R}^{(n_e \times n_e) \times 2H + n_e}$.

C. QUADRATIC OPERATOR Q (·, ·)

The quadratic operator $\boldsymbol{q}(\cdot, \cdot)$ in (14) can be written into the matrix form as follows,

$$
\boldsymbol{q}(\boldsymbol{X}, \boldsymbol{X}) = \begin{bmatrix} q_1 \\ \cdots \\ q_{n_e} \end{bmatrix} = \begin{bmatrix} \boldsymbol{X}^T \mathbb{A}_1 \boldsymbol{X} \\ \cdots \\ \boldsymbol{X}^T \mathbb{A}_{n_e} \boldsymbol{X} \end{bmatrix}, \quad (25)
$$

where $\mathbb{A}_i \in \mathbb{R}^{n_e \times n_e}, i \in \{1, 2, \ldots, n_e\}$ indicate specific constant matrixes corresponding to the detail of operator q_i

in (14). Substituting the harmonic solution (15) into (25), one obtains,

$$
\begin{bmatrix} q_1 \\ \cdots \\ q_k \\ \cdots \\ q_{n_e} \end{bmatrix} = \begin{bmatrix} \left(\boldsymbol{x}_0^T + \cdots + \boldsymbol{x}_H^T\right) \mathbb{A}_1 \left(\boldsymbol{x}_0 + \cdots + \boldsymbol{x}_H\right) \\ \cdots \\ \left(\boldsymbol{x}_0^T + \cdots + \boldsymbol{x}_H^T\right) \mathbb{A}_k \left(\boldsymbol{x}_0 + \cdots + \boldsymbol{x}_H\right) \\ \cdots \\ \left(\boldsymbol{x}_0^T + \cdots + \boldsymbol{x}_H^T\right) \mathbb{A}_{n_e} \left(\boldsymbol{x}_0 + \cdots + \boldsymbol{x}_H\right) \end{bmatrix},
$$

$$(26)$$

where $q_k, k \in \{1, 2, \ldots, n_e\}$ has general expression as follows,

$$
q_k = \left(\boldsymbol{x}_0^T + \cdots + \boldsymbol{x}_H^T\right) \mathbb{A}_k \left(\boldsymbol{x}_0 + \cdots + \boldsymbol{x}_H\right)
$$

$$
= \left(\boldsymbol{x}_0^T \mathbb{A}_k + \cdots + \boldsymbol{x}_H^T \mathbb{A}_k\right) \left(\boldsymbol{x}_0 + \cdots + \boldsymbol{x}_H\right)
$$

$$
= \underbrace{\boldsymbol{x}_1^T \mathbb{A}_k \boldsymbol{x}_0 + \cdots + \boldsymbol{x}_H^T \mathbb{A}_k \boldsymbol{x}_0}_{\sum_{i=1}^{H} q_k(\boldsymbol{x}_i, \boldsymbol{x}_0)} + \underbrace{\boldsymbol{x}_0^T \mathbb{A}_k \boldsymbol{x}_1 + \cdots + \boldsymbol{x}_0^T \mathbb{A}_k \boldsymbol{x}_H}_{\sum_{i=1}^{H} q_k(\boldsymbol{x}_0, \boldsymbol{x}_i)}
$$

$$
+ \underbrace{\boldsymbol{x}_0^T \mathbb{A}_k \boldsymbol{x}_0}_{q_k(\boldsymbol{x}_0, \boldsymbol{x}_0)} + \underbrace{\boldsymbol{x}_1^T \mathbb{A}_k \boldsymbol{x}_1 + \boldsymbol{x}_1^T \mathbb{A}_k \boldsymbol{x}_2 + \cdots + \boldsymbol{x}_i^T \mathbb{A}_k \boldsymbol{x}_j + \cdots}_{\sum_{i=1}^{H} \sum_{j=1}^{H} q_k(\boldsymbol{x}_i, \boldsymbol{x}_j)}.
$$

$$(27)$$

In the four parts of (27), the third item in (27) can only generate constant bias as follows,

$$
q_k(\boldsymbol{x}_0, \boldsymbol{x}_0) = \boldsymbol{x}_0^T \mathbb{A}_k \boldsymbol{x}_0 = \boldsymbol{a}^T \mathbb{A}_k \boldsymbol{a}. \quad (28)
$$

The first and second item in (27) can only generate integer harmonic as follows,

$$
\sum_{i=1}^{H} q_k(\boldsymbol{x}_0, \boldsymbol{x}_i) = \sum_{i=1}^{H} \boldsymbol{a}^T \mathbb{A}_k \boldsymbol{b}_i \cos i\boldsymbol{\omega}t + \sum_{i=1}^{H} \boldsymbol{a}^T \mathbb{A}_k \boldsymbol{c}_i \sin i\boldsymbol{\omega}t
$$

$$
\sum_{i=1}^{H} q_k(\boldsymbol{x}_i, \boldsymbol{x}_0) = \sum_{i=1}^{H} \boldsymbol{a}^T \mathbb{A}_k^T \boldsymbol{b}_i \cos i\boldsymbol{\omega}t + \sum_{i=1}^{H} \boldsymbol{a}^T \mathbb{A}_k^T \boldsymbol{c}_i \sin i\boldsymbol{\omega}t.
$$

$$(29)$$

The general expression of the fourth term in (27) can be formulated as follows,

$$
q_k(\boldsymbol{x}_i, \boldsymbol{x}_j)
$$

$$
= \boldsymbol{x}_i^T \mathbb{A}_k \boldsymbol{x}_j
$$

$$
= (\boldsymbol{b}_i \cos i\boldsymbol{\omega}t + \boldsymbol{c}_i \sin i\boldsymbol{\omega}t)^T \times \mathbb{A}_k (\boldsymbol{b}_j \cos j\boldsymbol{\omega}t + \boldsymbol{c}_j \sin j\boldsymbol{\omega}t)
$$

$$
= \cos\left(i\boldsymbol{\omega}^T t\right) \boldsymbol{b}_i^T \mathbb{A}_k \boldsymbol{b}_j \cos j\boldsymbol{\omega}t + \cos\left(i\boldsymbol{\omega}^T t\right) \boldsymbol{b}_i^T \mathbb{A}_k \boldsymbol{c}_j \sin j\boldsymbol{\omega}t
$$

$$
+ \sin\left(i\boldsymbol{\omega}^T t\right) \boldsymbol{c}_i^T \mathbb{A}_k \boldsymbol{b}_j \cos j\boldsymbol{\omega}t + \sin\left(i\boldsymbol{\omega}^T t\right) \boldsymbol{c}_i^T \mathbb{A}_k \boldsymbol{c}_j \sin j\boldsymbol{\omega}t
$$

$$
+ \text{HCT}, \quad (30)
$$

where the harmonic crossing term (HCT) mainly produces non-integer sub-harmonics.

Because of the natural low-pass filtering characteristic of second order Kuramoto model, non-integer sub-harmonics only have limited influence to the approximate solution.

Thus, the forms by ignoring the HCT of the fourth term in (27) according to (30) can be obtained as follows,

$$\sum_{i=1}^{H}\sum_{j=1}^{H} q_k(\boldsymbol{x}_i, \boldsymbol{x}_j)$$

$$\approx q_{0,k} + \sum_{j=1}^{H}\left(\boldsymbol{q}_{cj,k}^T \cos j\boldsymbol{\omega}t + \boldsymbol{q}_{sj,k}^T \sin j\boldsymbol{\omega}t\right), \quad (31)$$

where $q_{0,k} \in \mathbb{R}$, $\boldsymbol{q}_{cj,k} \in \mathbb{R}^{n_e}$, and $\boldsymbol{q}_{sj,k} \in \mathbb{R}^{n_e}$ are expressed as follows,

$$q_{0,k} = \sum_{i=1}^{H} \frac{1}{2}\left[\left(diag\left(\boldsymbol{b}_i^T \mathbb{A}_k \boldsymbol{b}_i + \boldsymbol{c}_i^T \mathbb{A}_k \boldsymbol{c}_i\right)\right)^T \cdot \boldsymbol{1}\right] \quad (32)$$

$$\boldsymbol{q}_{cj,k} = \sum_{\substack{i=1;\& \\ 1\le i-j\le H}}^{H}\left[\frac{1}{2}\left(diag\left(\boldsymbol{b}_i^T \mathbb{A}_k \boldsymbol{b}_{i-j} + \boldsymbol{c}_i^T \mathbb{A}_k \boldsymbol{c}_{i-j}\right)\right)\right]$$

$$+ \sum_{\substack{i=1;\& \\ 1\le i+j\le H}}^{H}\left[\frac{1}{2}\left(diag\left(\boldsymbol{b}_i^T \mathbb{A}_k \boldsymbol{b}_{i+j} + \boldsymbol{c}_i^T \mathbb{A}_k \boldsymbol{c}_{i+j}\right)\right)\right],$$

$$\quad (33)$$

$$+ \sum_{\substack{i=1;\overline{\jmath};\& \\ 1\le j\le i\le H}}\left[\frac{1}{2}\left(diag\left(\boldsymbol{b}_i^T \mathbb{A}_k b_{j-i} - \boldsymbol{c}_i^T \mathbb{A}_k \boldsymbol{c}_{j-i}\right)\right)\right]$$

$$\boldsymbol{q}_{sj,k} = \sum_{\substack{i=1; \\ 1\le i-j\le H}}^{H}\left[\frac{1}{2}\left(diag\left(\boldsymbol{c}_i^T \mathbb{A}_\hbar \boldsymbol{b}_{i-j} - \boldsymbol{b}_i^T \mathbb{A}_k \boldsymbol{c}_{i-j}\right)\right)^T\right]$$

$$+ \sum_{\substack{i=1;\& \\ 1\le i+j\le H}}^{H}\left[\frac{-1}{2}\left(diag\left(\boldsymbol{c}_i^T A_\hbar \boldsymbol{b}_{i+j} - \boldsymbol{b}_i^T \mathbb{A}_k \boldsymbol{c}_{i+j}\right)\right)^T\right],$$

$$+ \sum_{\substack{i=1;\& \\ 1\le j-i\le H}}^{H}\left[\frac{1}{2}\left(diag\left(\boldsymbol{b}_i^T \mathbb{A}_k \boldsymbol{c}_{j-i} + \boldsymbol{c}_i^T \mathbb{A}_k \boldsymbol{b}_{j-i}\right)\right)^T\right]$$

$$\quad (34)$$

where the symbol $diag(\cdot)$ represent to take matrix diagonal operation. Combining (28), (29), and (31), $\boldsymbol{q}(\boldsymbol{X}, \boldsymbol{X})$ in (25) can be formulated as follows,

$$\boldsymbol{q}(\boldsymbol{X}, \boldsymbol{X}) \approx \boldsymbol{p}_0 + \sum_{k=1}^{H}\boldsymbol{p}_{c,k} \cos(k\boldsymbol{\omega}t) + \sum_{k=1}^{H}\boldsymbol{p}_{s,k}\sin(k\boldsymbol{\omega}t), \quad (35)$$

where each coefficient in (35) of is demonstrated as follows,

$$\boldsymbol{p}_0^T = \left[\boldsymbol{a}^T \mathbb{A}_1 \boldsymbol{a} + q_{0,1} \cdots \boldsymbol{a}^T \mathbb{A}_{n_e}\boldsymbol{a} + q_{0,n_e}\right]^T$$

$$\boldsymbol{p}_{c,k} = \begin{bmatrix} \boldsymbol{q}_{ck,1}^T + \boldsymbol{a}^T\left(\mathbb{A}_1^T + \mathbb{A}_1\right)\boldsymbol{b}_k \\ \cdots \\ \boldsymbol{q}_{ck,n_e}^T + \boldsymbol{a}^T\left(\mathbb{A}_{n_e}^T + \mathbb{A}_{n_e}\right)\boldsymbol{b}_k \end{bmatrix}$$

$$\boldsymbol{p}_{s,k} = \begin{bmatrix} \boldsymbol{q}_{sk,1}^T + \boldsymbol{a}^T\left(\mathbb{A}_1^T + \mathbb{A}_1\right)\boldsymbol{c}_k \\ \cdots \\ \boldsymbol{q}_{sk,n_e}^T + \boldsymbol{a}^T\left(\mathbb{A}_{n_e}^T + \mathbb{A}_{n_e}\right)\boldsymbol{c}_k \end{bmatrix}. \quad (36)$$

Hence, the expression of $\boldsymbol{Q}(\boldsymbol{U}, \boldsymbol{U})$ in (17) according to (25) can be formulated as follows,

$$\boldsymbol{Q}(\boldsymbol{U}, \boldsymbol{U}) = \begin{bmatrix} \boldsymbol{p}_0^T, \mathbf{row}\left(\boldsymbol{p}_{c,1}\right)^T, \mathbf{row}\left(\boldsymbol{p}_{s,1}\right)^T, \cdots \\ \cdots, \mathbf{row}\left(\boldsymbol{p}_{c,H}\right)^T, \mathbf{row}\left(\boldsymbol{p}_{s,H}\right)^T \end{bmatrix}^T. \quad (37)$$

D. EXPLICIT EXPRESSION OF HARMONIC ALGEBRAIC EQUATION

Simultaneous (21), (22), (24) and (37), an explicit HAE of (17) can be obtained as follows,

$$\begin{bmatrix} 0 \\ \mathbf{row}\left(Y_{c,1}\right) \\ \mathbf{row}\left(Y_{s,1}\right) \\ \cdots \\ \mathbf{row}\left(Y_{c,H}\right) \\ \mathbf{row}\left(Y_{s,H}\right) \end{bmatrix} = \begin{bmatrix} c \\ 0 \\ 0 \\ \cdots \\ 0 \\ 0 \end{bmatrix} + \begin{bmatrix} \mathbb{L}a \\ \mathbf{row}\left(\mathbb{L}b_1\right) \\ \mathbf{row}\left(\mathbb{L}c_1\right) \\ \cdots \\ \mathbf{row}\left(\mathbb{L}b_H\right) \\ \mathbf{row}\left(\mathbb{L}c_H\right) \end{bmatrix} + \begin{bmatrix} p_0 \\ \mathbf{row}\left(p_{c,k}\right) \\ \mathbf{row}\left(p_{s,k}\right) \\ \cdots \\ \mathbf{row}\left(p_{c,H}\right) \\ \mathbf{row}\left(p_{s,H}\right) \end{bmatrix} \quad (38)$$

Simultaneous (18) and (38) can be solved numerically, through the conventional iterative method, such as the Newton method.

IV. HARMONIC SOLUTION OF SECOND ORDER KURAMOTO OSCILLATOR MODEL

In this section, the pure differential equations described in section II is converted into a QDAE system, technically, by introducing auxiliary variables in Section IV-A and the coefficients matrices related to QDAE is derived later.

A. THE QDAE OF SECOND ORDER KURAMOTO OSCILLATOR MODEL

Considering the weak damping property of power system [32], the damping coefficient in (13) is set to zero, i.e., $\mu = 0$. A set of auxiliary variables is introduced as follows,

$$\begin{cases} \boldsymbol{w}_2 = diag\left(\boldsymbol{\alpha}\boldsymbol{z}_1\right)\boldsymbol{\alpha}\boldsymbol{z}_1 \\ \boldsymbol{w}_4 = [diag\left(\boldsymbol{\alpha}\boldsymbol{z}_1\right)]^3 \boldsymbol{\alpha}\boldsymbol{z}_1 \\ \boldsymbol{w}_6 = [diag\left(\boldsymbol{\alpha}\boldsymbol{z}_1\right)]^5 \boldsymbol{\alpha}\boldsymbol{z}_1. \end{cases} \quad (39)$$

Denoting $\boldsymbol{z}'_1 = \boldsymbol{\varpi}$, (13)-(I) can be formulated as a QDAE system as follows,

where $\boldsymbol{X} = [\boldsymbol{z}_1, \boldsymbol{\varpi}, \boldsymbol{w}_2, \boldsymbol{w}_4, \boldsymbol{w}_6]$, $\boldsymbol{X} \in \mathbb{R}^{n_e \times 1}$, $n_e = 2n + 3N_\alpha$, and the symbol $\circ$ denotes the Hadamard product of vectors.

B. EXPLICIT MATRIX COEFFICIENT OF OPERATOR

We now focus on $\boldsymbol{q}(\boldsymbol{X}, \boldsymbol{X})$ in (40), as shown at the bottom of the next page. Expanding matrix $\boldsymbol{\alpha} = (\alpha_{ij}) \in \mathbb{R}^{n_\alpha \times n}$ and vector $\boldsymbol{z}_1 = (z_{ij}) \in \mathbb{R}^{n \times 1}$, one obtains,

$$-(\boldsymbol{\alpha}\boldsymbol{z}_1) \circ (\boldsymbol{\alpha}\boldsymbol{z}_1) = \begin{bmatrix} \boldsymbol{z}_1^T \boldsymbol{b}_{2,1}\boldsymbol{z}_1 \\ \cdots \\ \cdots \\ \boldsymbol{z}_1^T \boldsymbol{b}_{2,n_\alpha}\boldsymbol{z}_1 \end{bmatrix} = \begin{bmatrix} \boldsymbol{X}^T \boldsymbol{B}_{2,1}\boldsymbol{X} \\ \cdots \\ \cdots \\ \boldsymbol{X}^T \boldsymbol{B}_{2,n_\alpha}\boldsymbol{X} \end{bmatrix}, \quad (41)$$

where $b_{2,k} = -[\alpha(k,:)]^T \alpha(k,:)$, $b_{2,k} \in \mathbb{R}^{n \times n}$, and the symbol $\alpha(k,:)$ represents the k-th row of matrix α. Furthermore, the following equation holds,

$$\underbrace{\sigma_1 A_3}_{C_3} (w_2 \circ (\alpha z_1)) = \begin{bmatrix} z_1^T b_{3,1} w_2 \\ \cdots \\ \cdots \\ z_1^T b_{3,n} w_2 \end{bmatrix} = \begin{bmatrix} X^T B_{3,1} X \\ \cdots \\ \cdots \\ X^T B_{3,n} X \end{bmatrix},$$

(42)

where $b_{3,k} = \alpha^T diag(C_3(k,:))$, $b_{2,k} \in \mathbb{R}^{n \times n_\alpha}$. Moreover, one obtains,

$$\underbrace{\sigma_1 A_5}_{C_5} (w_4 \circ (\alpha z_1)) = \begin{bmatrix} z_1^T b_{5,1} w_4 \\ \cdots \\ \cdots \\ z_1^T b_{5,n} w_4 \end{bmatrix} = \begin{bmatrix} X^T B_{5,1} X \\ \cdots \\ \cdots \\ X^T B_{5,n} X \end{bmatrix},$$

(43)

$$\underbrace{\sigma_1 A_7}_{C_7} (w_6 \circ (\alpha z_1)) = \begin{bmatrix} z_1^T b_{7,1} w_6 \\ \cdots \\ \cdots \\ z_1^T b_{7,n} w_6 \end{bmatrix} = \begin{bmatrix} X^T B_{7,1} X \\ \cdots \\ \cdots \\ X^T B_{7,n} X \end{bmatrix},$$

(44)

where $b_{7,k} = \alpha^T diag(C_7(k,:))$, $b_{5,k} = \alpha^T diag(C_5(k,:))$. The corresponding matrices appeared in (41), (42), (43) and (44) can be written as follows,

$$B_{2,k} = \begin{bmatrix} b_{2,k} & 0 \\ 0 & 0 \end{bmatrix}; \qquad B_{3,k} = \begin{bmatrix} 0 & b_{3,k} & 0 & 0 \\ 0 & 0 & 0 & 0 \end{bmatrix},$$
$$B_{5,k} = \begin{bmatrix} 0 & 0 & b_{5,k} & 0 \\ 0 & 0 & 0 & 0 \end{bmatrix}; B_{7,k} = \begin{bmatrix} 0 & 0 & 0 & b_{7,k} \\ 0 & 0 & 0 & 0 \end{bmatrix},$$

(45)

where 0 indicates a full 0 vector of appropriate dimension, and $B_{\{2,3,5,7\},k} \in \mathbb{R}^{n_e \times n_e}$. Denoting $w_2 = (w_{2,i}) \in \mathbb{R}^{n_\alpha \times 1}$, it is easily seen that,

$$-w_2 \circ w_2 = \begin{bmatrix} w_2^T k_{1,1} w_2 \\ \cdots \\ \cdots \\ w_2^T k_{1,n_\alpha} w_2 \end{bmatrix} = \begin{bmatrix} X^T K_{1,1} X \\ \cdots \\ \cdots \\ X^T K_{1,n_\alpha} X \end{bmatrix}, \quad (46)$$

where $k_{1,k} \in \mathbb{R}^{n_\alpha \times n_\alpha}$, all elements of the matrix are equal to zero except the position (k,k) is equal to -1. Analogously,

the following equation holds,

$$-w_2 \circ w_4 = \begin{bmatrix} w_2^T k_{2,1} w_4 \\ \cdots \\ \cdots \\ w_2^T k_{2,n_\alpha} w_4 \end{bmatrix} = \begin{bmatrix} X^T K_{2,1} X \\ \cdots \\ \cdots \\ X^T K_{2,n_\alpha} X \end{bmatrix}, \quad (47)$$

where $k_{2,k} \in \mathbb{R}^{n_\alpha \times n_\alpha}$ has a structure identical to that of $k_{1,k}$. Similarly, we have,

$$K_{1,k} = \begin{bmatrix} 0 & 0 & 0 & 0 \\ 0 & k_{1,k} & 0 & 0 \\ 0 & 0 & 0 & 0 \end{bmatrix};$$
$$K_{2,k} = \begin{bmatrix} 0 & 0 & 0 & 0 \\ 0 & 0 & k_{2,k} & 0 \\ 0 & 0 & 0 & 0 \end{bmatrix},$$

(48)

where $K_{\{1,2\},k} \in \mathbb{R}^{n_e \times n_e}$.

Denoting $q(X,X) = [q_1, q_2, q_3, q_4, q_5]$ and combining (41), (42), (43), (44), (46) and (47), the coefficient matrixes $\mathbb{A}_k$, $k \in \{n, \ldots, 2n + 3n_\alpha\}$ are shown as follows,

$$q_2 = \begin{bmatrix} X^T \underbrace{(B_{3,1} + B_{5,1} + B_{7,1})}_{\mathbb{A}_{n+1}} X \\ \cdots \\ X^T \underbrace{(B_{3,n} + B_{5,n} + B_{7,n})}_{\mathbb{A}_{2n}} X \end{bmatrix} \quad q_3 = \begin{bmatrix} X^T \underbrace{B_{2,1}}_{\mathbb{A}_{2n+1}} X \\ \cdots \\ X^T \underbrace{B_{2,n_\alpha}}_{\mathbb{A}_{2n+n_\alpha}} X \end{bmatrix},$$

(49)

$$q_4 = \begin{bmatrix} X^T \underbrace{K_{1,1}}_{\mathbb{A}_{2n+n_\alpha+1}} X \\ \cdots \\ X^T \underbrace{K_{1,n_\alpha}}_{\mathbb{A}_{2n+2n_\alpha}} X \end{bmatrix}; \quad q_5 = \begin{bmatrix} X^T \underbrace{K_{2,1}}_{\mathbb{A}_{2n+2n_\alpha+1}} X \\ \cdots \\ X^T \underbrace{K_{2,n_\alpha}}_{\mathbb{A}_{2n+3n_\alpha}} X \end{bmatrix},$$

(50)

where $\mathbb{A}_k = 0$, $k \in \{1, 2, \cdots, n\}$.

Analogously, the coefficient matrix $\mathbb{L}$, $\mathbb{D}$ and C corresponding to $m(X')$, $l(X)$, c in (40) are shown as follows,

$$\mathbb{L} = \begin{bmatrix} 0 & 1 & & & \\ -\lambda^2 & 0 & \sigma_1 A_2 & \sigma_1 A_4 & \sigma_1 A_6 \\ & 1 & & & \\ & & & 1 & \\ & & & & 1 \end{bmatrix}.$$

$$\begin{aligned}
z'_1 &= \varpi \\
\varpi' &= -\lambda^2 z_1 + \sigma_1 A_2 w_2 + \sigma_1 A_4 w_4 + \sigma_1 A_6 w_6 && + \sigma_1 A_3 (w_2 \circ (\alpha z_1)) + \sigma_1 A_5 (w_4 \circ (\alpha z_1)) + \sigma_1 A_7 (w_6 \circ (\alpha z_1)) \\
0 &= w_2 && - (\alpha z_1) \circ (\alpha z_1) \\
0 &= w_4 && - w_2 \circ w_2 \\
\underbrace{0}_{m(X')} &= \underbrace{w_6}_{l(X)} && - \underbrace{w_2 \circ w_4}_{q(X,X)},
\end{aligned}$$

(40)

$$\mathbb{D} = \begin{bmatrix} 1 & & & & \\ & 1 & & & \\ & & 0 & & \\ & & & 0 & \\ & & & & 0 \end{bmatrix}; \qquad C = \begin{bmatrix} 0 \\ 0 \\ 0 \\ 0 \\ 0 \end{bmatrix}. \quad (51)$$

So far we get all the coefficient matrices $\mathbb{A}_k$, $\mathbb{L}$, $\mathbb{D}$, C of the (40), thus the HAE can be formulated according to (38) aiming to obtain the harmonic solution of (13)-(I).

V. ANALYSIS OF THE SECOND ORDER KURAMOTO OSCILLATOR NETWORK

This section analyses the solution structure of Kuramoto oscillator network via obtained harmonic solution. Then the relative motion equation of oscillators in Kuramoto network is concluded by a set of nonlinear state output equations. Finally, a phase-domain margin index is proposed to assess the stability of oscillator system quantitatively.

A. THE SOLUTION STRUCTURE OF THE KURAMOTO OSCILLATOR NETWORK

For ease of analysis, supposing that the order of harmonics is equal to 1, i.e., $H = 1$, and assuming that the HAE (38) can be solved numerically. The harmonic solution of the second order Kuramoto oscillator network is simplified as follows,

$$z_1(t) = a + b_1 \cos \omega t + c_1 \sin \omega t + \text{HHT}$$
$$\approx a + M_{bc} \times \cos(\omega t + \varphi), \quad (52)$$

where a is constant vector, M_{bc} is the amplitude matrix, and φ is the initial phase vector. Higher harmonic terms (HHT) represent those harmonics with order greater than 1. Plugging (52) into (13)-(II) with zero-damping assumption, one can obtain as follows,

$$z''_{n+1} = \sum_{k=2}^{7} \left(\sigma_2 A_k \left[diag\left(\alpha z_1\right)\right]^{k-1} \alpha z_1 \right) = f_{nl}(z_1(t))$$
$$= 2k_2 - a_2 \bar{\omega}^2 \cos(\bar{\omega} t + \varphi_{20}) + \text{HHT}, \quad (53)$$

where k_2, a_2, φ_{20}, and $\bar{\omega}$ are the constant determined by the nonlinear function $f_{nl}(\cdot)$.

Neglecting HHT and integrating (53) the first-order harmonic approximate solution of (53) can be obtained as follows,

$$z_{n+1}(t) = k_2 t^2 + C_1 t + C_0 + a_2 \cos(\bar{\omega} t + \varphi_{20}) + \text{HHT}, \quad (54)$$

where C_0, C_1 are the integral constants determined by the initial value condition in (53). The analytical solution in y coordinate system can be formulated by using the inverse transformation as follows,

$$y = \mathcal{U}z = [u, 1] \begin{bmatrix} z_1(t) \\ z_{n+1}(t) \end{bmatrix} = uz_1(t) + z_{n+1}(t)$$
$$\approx \underbrace{k_2 t^2 + C_1 t + C_0 + ua}_{y_s}$$

$$+ \underbrace{uM_{bc} \cos(\omega t + \varphi) + a_2 \cos(\bar{\omega} t + \varphi_{20})}_{y_o} = y_s + y_o. \quad (55)$$

It can be seen from (55) that the solution of second order Kuramoto oscillator network can be decomposed into two parts. One part is the multi-harmonic oscillation motion y_o, that is non-zero eigenvalue part, which makes the phase angles of the whole network oscillate with each other, and the other is the acceleration motion component y_s, i.e., zero eigenvalue part, which pushes the phase angles of the whole network forward.

In particular, if one sets $\epsilon_3 = \epsilon_5 = \epsilon_7 = 0$, the nonlinear system (13) degenerates into a linear system as follows,

$$\begin{cases} z''_1 = -\lambda^2 z_1 & (I) \\ z''_{n+1} = 0 & (II). \end{cases} \quad (56)$$

And the approximate solution of (55) becomes exact solution of (56) as follows,

$$y = \mathcal{U}z = C_1 t + C_0 + uM_{bc} \cos(\omega t + \varphi). \quad (57)$$

Thus, previous discussion reveals that the zero eigenvalue of A_1 is related to the uniform motion of all oscillators, while the non-zero eigenvalues basically dedicate to the vibration among oscillators.

B. THE RELATIVE MOTION EQUATION OF OSCILLATORS IN KURAMOTO NETWORK

Denoting the transformation matrix $\mathcal{U}$ mentioned in (10) as $\mathcal{U}^T = [V_1^T, \cdots, V_j^T, \cdots, V_n^T, \cdots, V_{n+1}^T]$ with $V_i^T = [v_i^T, 1]$, the phase angle differences can be written as,

$$y_{ij} = y_i - y_j = \left(V_i^T - V_j^T \right) z$$
$$= \left[v_i^T - v_j^T, 0 \right] \begin{bmatrix} z_1(t) \\ z_{n+1}(t) \end{bmatrix} = \left(v_i - v_j \right)^T z_1(t). \quad (58)$$

Without loss of generality, we can set $j = n+1$, where $i = 1, 2, 3, \cdots, n$. The angle difference δ_Δ can be formulated as follows,

$$\delta_\Delta = \mathcal{V} \cdot z_1, \quad (59)$$

where, $\delta_\Delta = [y_{1,n+1}, y_{2,n+1}, \ldots, y_{n,n+1}]$ represents relative phase angle, and $\mathcal{V} = [v_1 - v_{n+1}, v_2 - v_{n+1}, \cdots, v_n - v_{n+1}]$ is the linear mapping matrix. Hence, it can be observed that there exists a linear mapping between the relative angle δ_Δ and the state variable z_1 from mathematical perspective.

Combining (13)-(I) and (59), the relative motion equation of oscillators in Kuramoto network can be written as follows,

$$\begin{cases} \dot{\mathcal{X}} = -\mathcal{L} \cdot \mathcal{X} + h_{nl}(\mathcal{X}) & (I) \\ \delta_\Delta = \mathcal{C} \cdot \mathcal{X} & (II) \\ \mathcal{X}_0 = \left[\mathcal{U}^{-1} y(0); \mathcal{U}^{-1} \dot{y}(0) \right] & (III), \end{cases} \quad (60)$$

where $\mathcal{X} = [z_1, z_2, \cdots, z_n, \dot{z}_1, \dot{z}_2, \cdots, \dot{z}_n] \in \mathbb{R}^{2n}$ is the state variable, $\delta_\Delta \in \mathbb{R}^{n \times 1}$ is the output variable. $\mathcal{L} \in \mathbb{R}^{2n \times 2n}$ and $\mathcal{C} \in \mathbb{R}^{n \times 2n}$ are related constant matrix. Nonlinear function $h_{nl} : \mathbb{R}^{2n} \to \mathbb{R}^{2n}$ is a smooth mapping, and $\mathcal{U}y(0) = z(0)$, $\mathcal{U}\dot{y}(0) = \dot{z}(0)$.
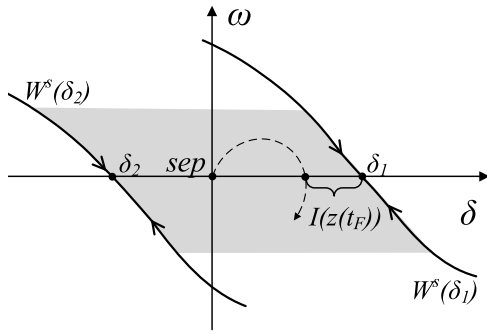
FIGURE 2. Stability boundary of single oscillator model.

C. A PHASE-DOMAIN STABILITY INDEX

The following celebrated result in the theory of stability region is relevant.

Theorem 1 ([32]): (Characterization of stability boundary): Consider an autonomous dynamic system $\dot{x} = f(x)$, let $x_i, i = 1, 2, 3, \cdots$ be the equilibrium points on the stability boundary $\partial A(x_s)$ of the SEP x_s. Under some mild assumptions, there is,

$$\partial A(x_s) = \cup W^s(x_i), \tag{61}$$

where $W^s(x_i)$ is the stable manifolds of x_i,

$$W^s(x_i) = \left\{ x \in \mathbb{R}^n : \lim_{t \to \infty} \phi(t, x) = x_i \right\}, \tag{62}$$

where $\phi(t, x)$ is the solution of $\dot{x} = f(x)$. $\square$

Consider a single oscillator model as follows,

$$M\ddot{\delta} = \Omega - D\dot{\delta} - a \sin \delta \tag{63}$$

The stability region of (63) can be shown in FIGURE 2. Theorem 1 above suggests that the boundary of the single oscillator model is composed of stable manifolds of $W^s(\delta_1)$ and $W^s(\delta_2)$. Hence, the phase-domain distance between the maximum of phase angle differences and the controlling UEP can be viewed as a numerical index to assess the stability margin of the second order Kuramoto oscillator network.

Therefore, a stability margin index can be defined as follows,

$$I(z(t_F)) = \left| \mathbf{Z}_{uep}(\mathcal{M}) - \max(z_{\mathcal{M}}(t)) \right|, \tag{64}$$

where $\mathcal{M} = \arg\max_{i \in N} |z_i(t)|$. $\mathbf{Z}_{uep} \in \mathbb{R}^{n \times 1}$ is the UEP of (13)-(I), i.e., $-\lambda^2 \mathbf{Z}_{uep} + \mathbf{g}_{nl}(\mathbf{Z}_{uep}) = \mathbf{0}$.

VI. CASE STUDY

In this section, several power system examples are employed as different second order Kuramoto oscillator network cases to show the effectiveness of QHBM and analysis.

A. SINGL MACHINE INFINITE BUSE POWER SYSTEM

Consider a single-machine infinite bus (SMIB) power system [34] with a diagram of topology as shown in FIGURE 3.
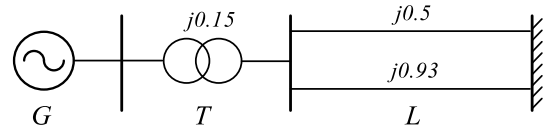

FIGURE 3. Diagram of the SMIB power system.

TABLE 1. The parameters of the SMIB power system.

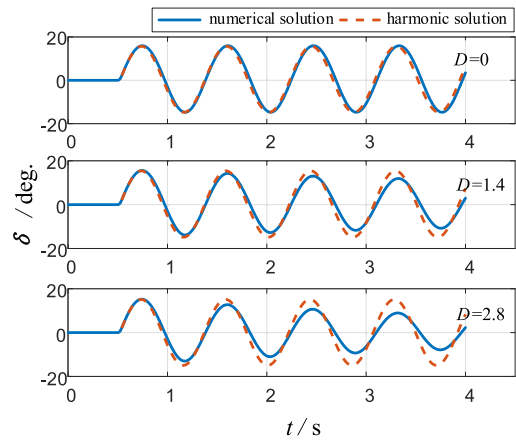| $\mathcal{H}$	D	P_M	$P_{\max}$	ω_R
3.5	0	0.9	1.35	376.8

FIGURE 4. Simulation of result with different damping coefficient and same fault duration time, i.e., $t_c = 0.06$ s.

The dynamics equation corresponding to SMIB system is shown as follows,

$$\begin{cases} \dfrac{2\mathcal{H}}{\omega_R}\ddot{\delta} + \dfrac{D}{\omega_R}\dot{\delta} = P_M - P_{\max} \sin \delta \\ \delta(t_c) = \delta_0; \quad \dot{\delta}(t_c) = \omega_0. \end{cases} \tag{65}$$

where the parameters in (65) are summarized in Table 1.

A three-phase short-circuit fault occurred at the generator terminal bus with fault durations time t_c equal to 0.06 s, and the response of SMIB power system with different damping coefficients are shown in FIGURE 4.

It can be observed that the harmonic solution fits the actual response of the SMIB power system well when the damping coefficient is set as zero, but this is not true when damping is not equal to 0. This demonstrates that the QHBM can only be applied to a zero-damping system, whose response is periodic. Moreover, the harmonic solutions with different selections of H are shown in FIGURE 5.

We can see that the performance of QHBM varies with different selection of H and t_c. Roughly speaking, depending on the harmonic composition of the actual solution and nonlinear degree of the SMIB system, the higher of order of harmonic, the more precise of harmonic solution. FIGURE 5 (a) shows that the performance of harmonic solution with H equal to 2 is much better than harmonic solution with H equal to 1 because of the consideration of a higher harmonic component in the
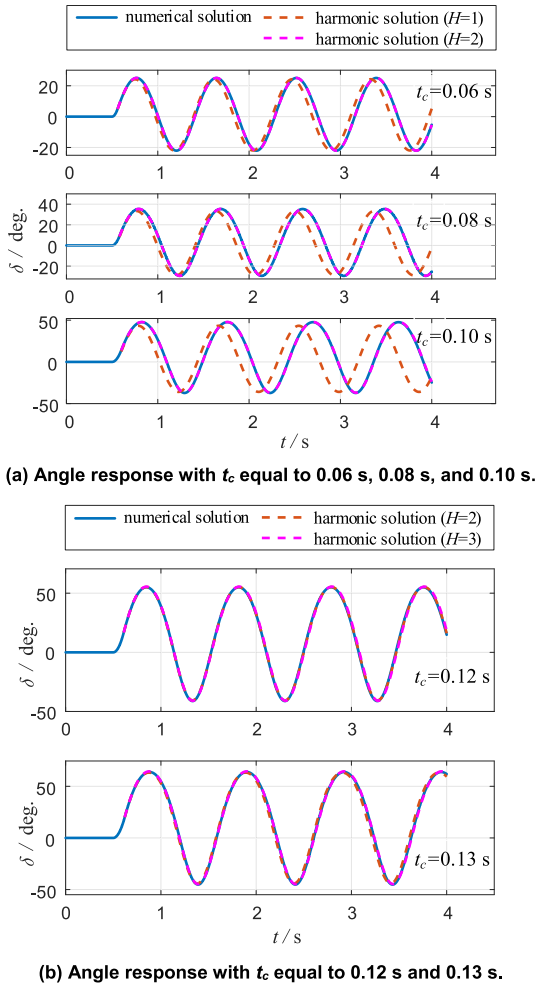
(a) Angle response with t_c equal to 0.06 s, 0.08 s, and 0.10 s.

(b) Angle response with t_c equal to 0.12 s and 0.13 s.

FIGURE 5. Simulation of result with different selection of *order of harmonic* and fault duration time.

former situation. The performance with H equal to 2, and 3 are almost the same from FIGURE 5 (b), which means that the third sub-harmonic component contributes very little in the actual solution.

Furthermore, taking H equal to 2 as an example, the analytical solution expression obtained by QHBM with t_c equal to 0.06 s is shown as follows,

$$
\begin{aligned}
y = {} & 0.0395 + 0.0347 \cos\left(7.1790 \times (t - 0.56)\right) \\
& + 0.4097 \sin\left(7.1790 \times (t - 0.56)\right) \\
& + 0.0130 \cos\left(2 \times 7.1790 \times (t - 0.56)\right) \\
& - 0.0023 \sin\left(2 \times 7.1790 \times (t - 0.56)\right),
\end{aligned} \tag{66}
$$

where $t \geq 0.56$. It can also be seen that the coefficient of second order sub-harmonics is quite smaller than the fundamental harmonics in (66), which means that the composition of the actual solution of SMIB system with t_c equal to 0.06 s includes virtually fundamental harmonics only. Moreover, the trend of the stability margin index with different fault duration times are shown in FIGURE 6.
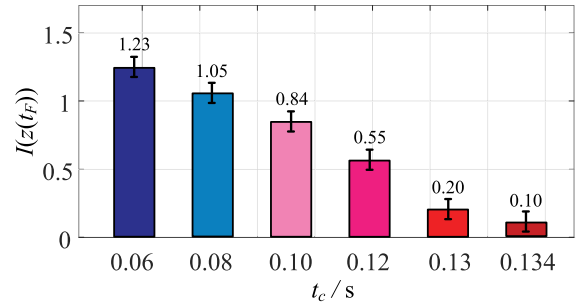
FIGURE 6. Trend of stability margin index with different t_c.
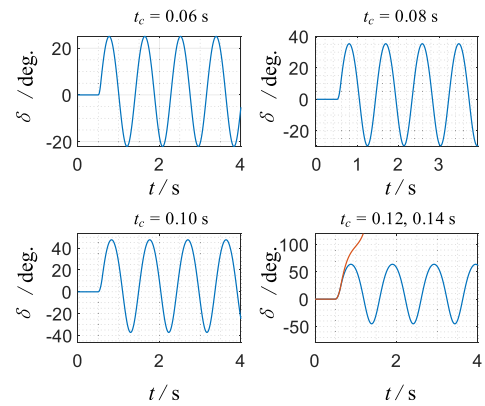
FIGURE 7. Phase angle responses of SMIB system. The blue curve represents stable response, while the red curve represents the unstable response.
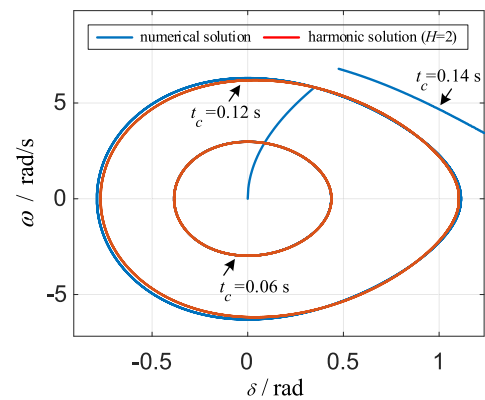

FIGURE 8. Phase portrait of SMIB power system.

From the FIGURE 6, we can infer that the critical fault time duration of SMIB system is 0.14 s around because of the nearness of stability margin index to zero as 0.134 s. In order to verify this inference, the response of SMIB power system with different fault time duration are shown in FIGURE 7.

Apparently, the time domain simulation indicates that the critical fault time duration is equal to 0.14 s from FIGURE 7 which coincides with the trend in FIGURE 6, demonstrating the effectiveness and accuracy of the phase domain index proposed in Section V-C. Furthermore, the phase portrait of
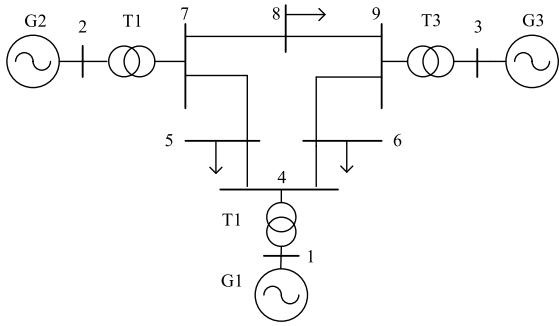
FIGURE 9. Diagram of IEEE 3-machine 9-bus power system.

SMIB system can be depicted through time domain simulation and harmonic solution as shown in FIGURE 8.

It can be seen that the harmonic solution fit the numerical solution very well even with fault time duration equal to 0.12 s from FIGURE 8. Moreover, the harmonic solution with t_c equal to 0.12 s is shown as follows,

$$
\begin{aligned}
y = {}& 0.2603 - 0.0044 \cos\left(6.1883 \times (t - 0.62)\right) \\
& + 0.9371 \sin\left(6.1883 \times (t - 0.62)\right) \\
& + 0.0926 \cos\left(2 \times 6.1883 \times (t - 0.62)\right) \\
& - 0.0013 \sin\left(2 \times 6.1883 \times (t - 0.62)\right), \qquad (67)
\end{aligned}
$$

where $t \geq 0.62$. Comparing (67) and (66), we can see that the constant harmonic a and fundamental harmonic amplitude increase as the nonlinear degree increase, indicating that the fundamental harmonic still is the main part of the approximate solution. This reflects, as previously asserted in (31), the low-pass filtering characteristics of second order Kuramoto model.

B. IEEE 3-MACHINE-9 BUS POWER SYSTEM

The diagram of the IEEE 3-machine 9-bus power system is shown in FIGURE 9, and the system parameters are obtained from reference [35].

The dynamic equation of the IEEE 3-machine 9-bus power system is a set of second order Kuramoto equations by setting $N = 2$ in (1), and the governed equation is shown as follows,

$$
\begin{cases}
\dfrac{2\mathcal{H}_i}{\omega_R}\ddot{\delta}_i + \underbrace{\dfrac{D_i}{\omega_R}}_{0}\dot{\delta}_i = P_{Mi} - \displaystyle\sum_{j=1}^{2+1} a_{ij} \sin\left(\delta_i - \delta_j - \gamma_{ij}\right) \\[4mm]
\delta_i(t_c) = \delta_{i,0}; \quad \dot{\delta}_i(t_c) = \omega_{i,0}; \qquad i = 1, 2, 3.
\end{cases}
$$

$$(68)$$

We set a three-phase short-circuit fault that occurred at bus 7 as a disturbance to (68), and the fault durations time is equal to 0.08 s. The angle responses of this Kuramoto oscillators network with zero-damping are shown in FIGURE 10.

Applying coordinate transformation $\boldsymbol{y} = \mathcal{U}\boldsymbol{z}$, the response in $\boldsymbol{Z}$ coordinate system of this power system can be obtained from FIGURE 10 (b). It can be seen that the phase angle responses in $\boldsymbol{Z}$ space can be divided into three parts, i.e., z_1, z_2
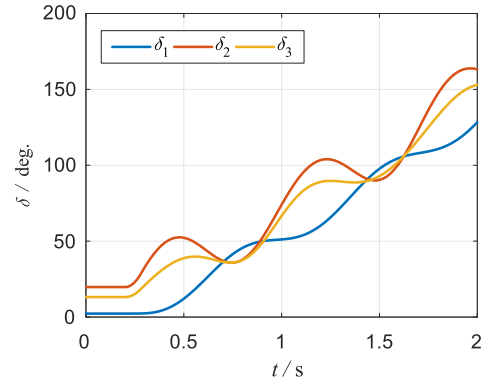
(a) Phase angle in δ coordinate system
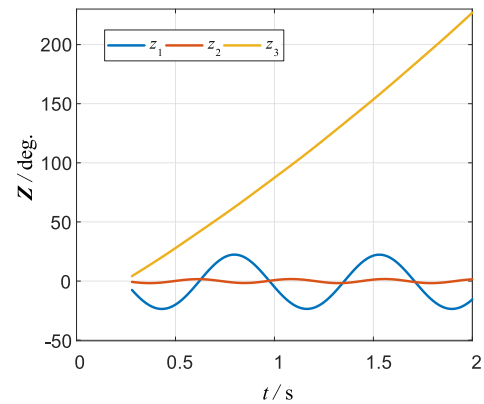
(b) Phase angle in $\boldsymbol{Z}$ coordinate system

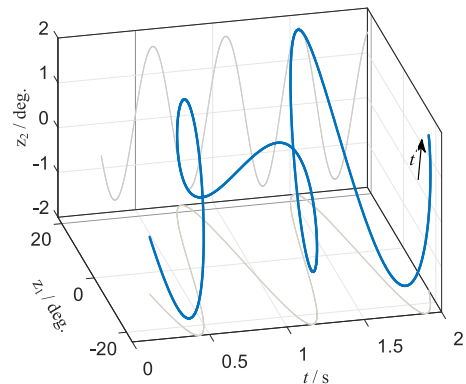**FIGURE 10.** Responses of phase angle in different coordinate system with tc equal to 0.08 s.

FIGURE 11. Response of nonlinear state variables z_1 and z_2.

and z_3, where the main subsystem variable z_1 and z_2 oscillates against each other, while the secondary subsystem variable z_3 shows the uniform motion characteristic, which validates the feasibility in Section V-A, explaining the morphological characteristics of oscillator's stable motions.

As can be seen from FIGURE 11, the projections of z_1 and z_2 in different directions can generate different oscillatory behaviors. Denoting $\boldsymbol{\mathcal{V}}^T = [\boldsymbol{v}_2 - \boldsymbol{v}_1, \boldsymbol{v}_3 - \boldsymbol{v}_1]$, the trajectories of the variables $\boldsymbol{\mathcal{V}}\boldsymbol{z}_1 = [y_{v2}, y_{v3}]$ are shown in FIGURE 12.
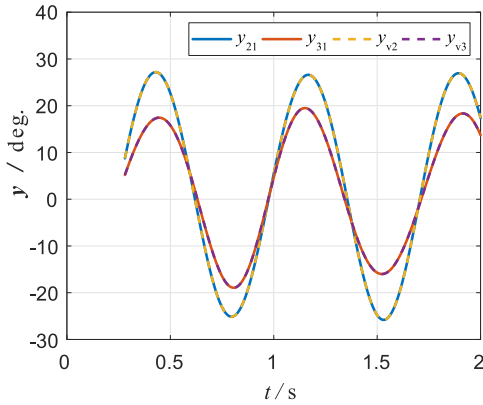
FIGURE 12. Diagram of relative angles. The solid curve is the subtraction of different phase angle, while the dashed curve is generated by (59).
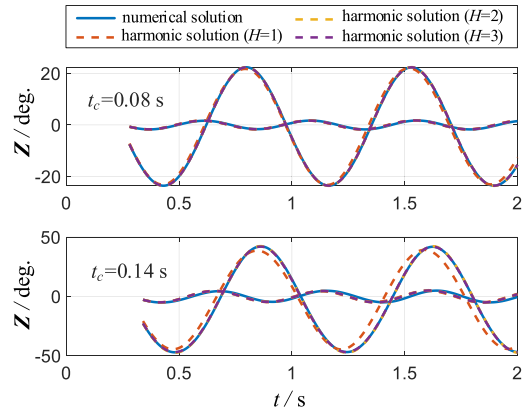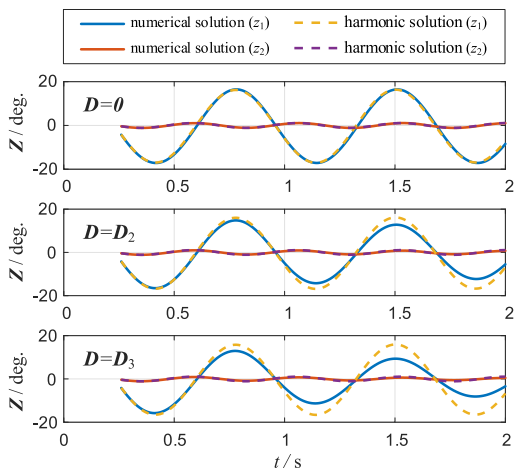

FIGURE 13. Simulation of result with different damping coefficient and same fault duration time, i.e., $t_c = 0.06$ s, where $D_2 = [21.27, 5.7, 2.7]$, and $D_3 = [42.5, 11.5, 5.4]$.
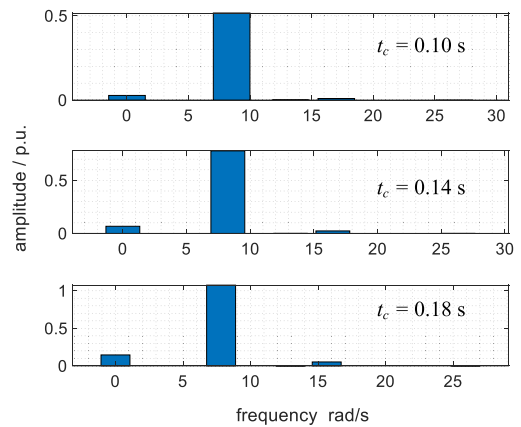

FIGURE 14. Simulation of result with different H and t_c.

FIGURE 15. Amplitude-frequency response of harmonic solution.

FIGURE 16. Phase angle responses with different tc. The solid line is numerical solution and the dash curve is harmonic solution with $H = 2$.

We see that the relative angle responses coincide with the new variables $\mathcal{V}z_1$ from FIGURE 12, demonstrating that (60) is capable of describing the relative motion of oscillator in Kuramoto network. The response of this power system with different damping coefficients are shown in FIGURE 13.

It can be concluded that QHBM can only be applied to dynamic system with zero-damping system from FIGURE 13 as illustrated in the SMIB system case. Besides, the comparison between numerical solution and harmonic solution with different selection of H is demonstrated in FIGURE 14.

It can be observed that the harmonic solution with H equal to 2 and 3 fits better than H equal to 1 both in the scenarios with $t_c = 0.08$ s and 0.14 s, respectively, from FIGURE 14, showing that the performance of solution with higher order of harmonic is better than lower order of harmonic.

FIGURE 15 demonstrates that the amplitude of constant harmonic a, fundamental harmonic and second order subharmonic is increased as fault time duration time increases, because of the harmonic distortion. This is consistent with the phenomenon in SMIB power system, further indicating
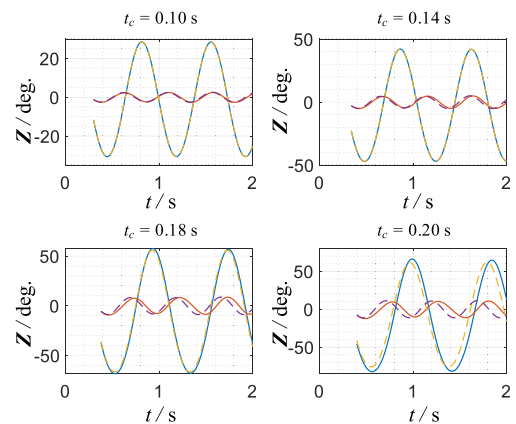
low-pass filtering characteristic of second order Kuramoto model asserted in (31).

Compared with the smaller amplitude component z_2, QHBM fit well in the larger amplitude component z_1 as fault time duration increases from FIGURE 16. Furthermore, the phase portrait of component z_1 is shown in FIGURE 17.
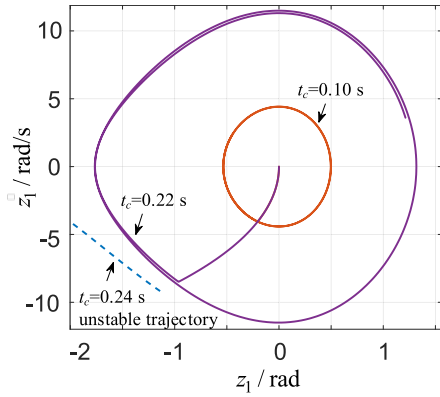
FIGURE 17. Phase portrait of IEEE 3-machine 9-bus system. The solid curve is obtained by QHBM and the dashed curve is numerical solution.
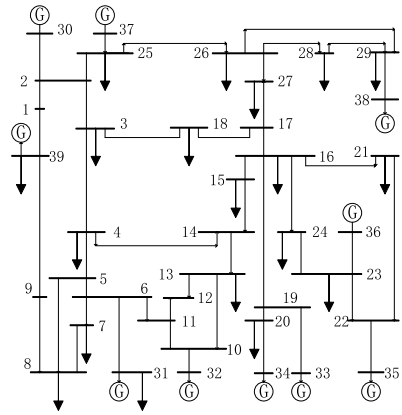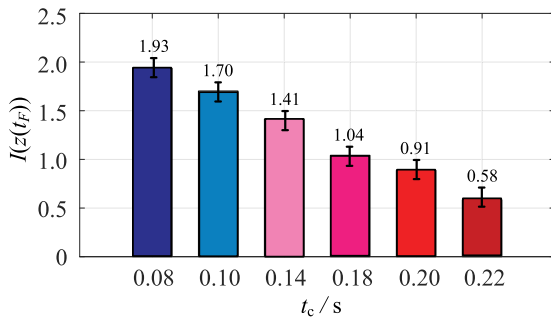

FIGURE 18. Stability margin index with different fault durations time.
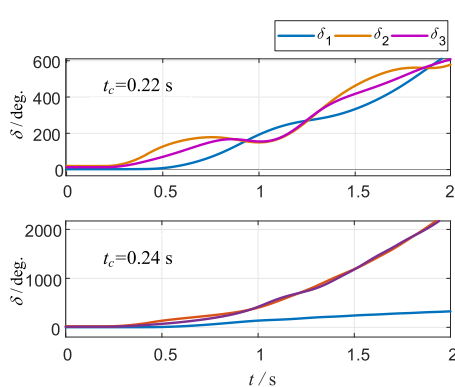
FIGURE 19. Simulation of result for power system with different t_c.

FIGURE 20. Diagram of IEEE 10-machine 39-bus power system.

(a) Rotor angle response in δ coordinate
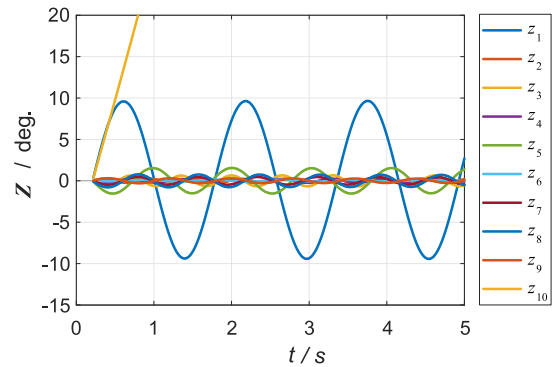

(b) Rotor angle response in Z coordinate

FIGURE 21. Responses of rotor angle in different coordinate system.

It can be seen that the phase portrait of z_1 is quite similar to the SMIB system portrait in FIGURE 17. We can infer that the critical fault time duration is between 0.22 s and 0.24 s. Hence, the distance between z_1 and the corresponding UEP can be viewed as a stability margin index according to (64). The variation of $I(z(t_F))$ versus fault time duration is shown in FIGURE 18.

From FIGURE 18, one can infer that the critical fault duration time is greater than 0.22 s, this observation is consistent with FIGURE 17, verifying the validity of (64). Moreover, the assertion can also be verified by the following time domain simulation in FIGURE 19.

The result in FIGURE 19 demonstrates that this power system keeps stable with t_c equal to 0.20 s while it loses stability with t_c equal to 0.24 s, indicating actual critical fault time duration time is between 0.22 s and 0.24 s, which is consistent with the assertion revealed by FIGURE 17 and 18.

C. IEEE 10-MACHINE 39-BUS POWER SYSTEM

The diagram of the IEEE 10-machine 39-bus system (a reduced-order system of the actual New England power
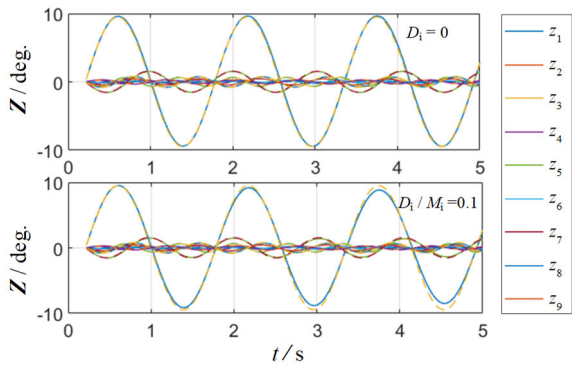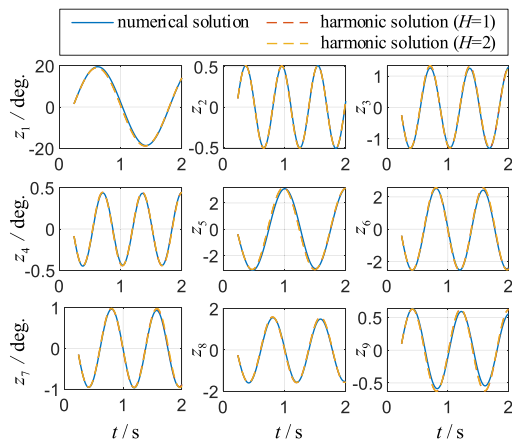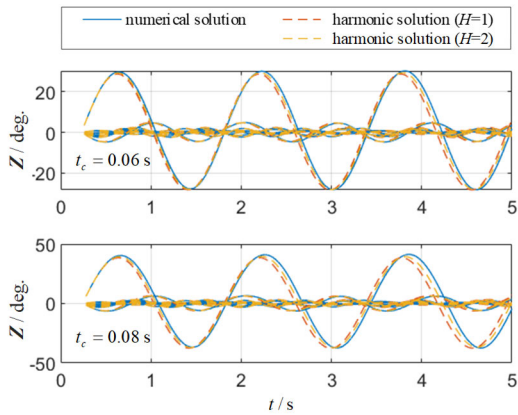
FIGURE 22. Simulation of result with different damping and same fault duration time and order of harmonic., i.e., $t_c = 0.06$ s, H= 1.

(a) Angle response with t_c equal to 0.04 s

(b) Angle response with t_c equal to 0.04 s and 0.08 s.

FIGURE 23. Comparison of numerical solution and harmonic solution.

system) is shown in FIGURE 20, and the system parameters are obtained from reference [36].

A three-phase short-circuit fault occurred, and the fault durations time is equal to 0.02 s. The responses of the rotor angle of the power system with non-damping are shown in FIGURE 21.

It can be seen that the rotor angle is moving forward after the clearance of fault in δ coordinate system from
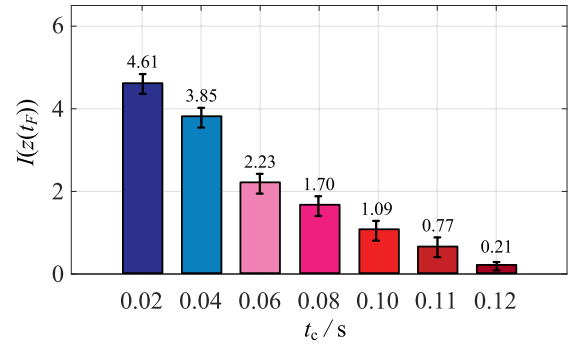

FIGURE 24. Stability margin index with different fault durations time.
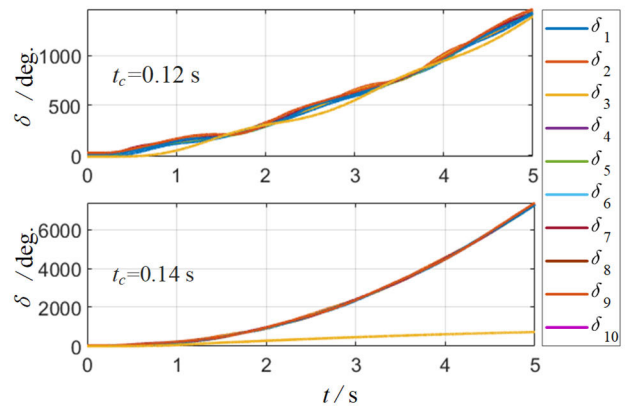

FIGURE 25. Time domain simulation for power system with different t_c.

FIGURE 21 (a), and those motions can be transformed into ten components in **Z** coordinate system, as uncovered by (13). The comparison between the numerical solution and harmonic solution with different damping conditions are shown in FIGURE 22.

FIGURE 22 shows that the harmonic solution in the zero-damping case fits better than damping case, which is consistent with the observation aforementioned. Furthermore, the comparison between numerical solution and harmonic solution with different order of harmonic are shown as follows.

FIGURE 23 demonstrates the performance of QHBM with different harmonic order and fault duration time. We can see that the performance of solution with H equal to 2 is better than the harmonic solution than $H = 1$ in general both in case with fault duration time equal to 0.06 s and 0.08, respectively. Furthermore, the variation of $I(z(t_F))$ versus fault time duration is shown in FIGURE 24.

FIGURE 24 demonstrates that the critical fault duration time is greater than 0.12 s, this inference can be examined by the time domain simulation as shown in FIGURE 25.

The result in FIGURE 25 manifests that the power system is stable with t_c equal to 0.12 s while it loses stability with t_c equal to 0.14 s, demonstrating that actual critical fault time duration time is between 0.12 s and 0.14 s, which is consistent

with the observation revealed by FIGURE 24. This result verifies the validity of the analysis in Section V.

VII. CONCLUSION

In this paper, a new polynomial model for the second order Kuramoto oscillator network is established. It is shown that the model can be partly decoupled by applying an eigen transformation. A new QHBM is proposed and derived in detail, and the harmonic solution by QHBM is efficient to estimate the actually response of the second order Kuramoto oscillator model with zero-damping. Based on the harmonic solution, the solution of Kuramoto oscillator model can be decomposed into two parts, i.e., multi-harmonic oscillation motion component and acceleration motion component, respectively, explaining the morphological characteristics of stable motion of oscillators in mathematic. The relative motion between different oscillators can be depicted by the proposed nonlinear state output equation system and large disturbance stability margin can be measure by phase domain stability index in this paper. Several power system cases used as different second order Kuramoto oscillator networks demonstrate the effectiveness and accuracy of the proposed approach and analysis.

REFERENCES

[1] Y. Kuramoto, "International symposium on mathematical problems in theoretical physics," *Lect. Notes Phys.*, vol. 30, pp. 420–422, 1975.

[2] A. Buscarino, L. V. Gambuzza, M. Porfiri, L. Fortuna, and M. Frasca, "Robustness to noise in synchronization of complex networks," *Sci. Rep.*, vol. 3, no. 1, pp. 1–6, Jun. 2013.

[3] G. Yang, D. Tong, Q. Chen, and W. Zhou, "Fixed-time synchronization and energy consumption for kuramoto-oscillator networks with multilayer distributed control," *IEEE Trans. Circuits Syst. II, Exp. Briefs*, vol. 70, no. 4, pp. 1555–1559, Apr. 2023.

[4] A. Parihar, N. Shukla, S. Datta, and A. Raychowdhury, "Exploiting synchronization properties of correlated electron devices in a non-Boolean computing fabric for template matching," *IEEE J. Emerg. Sel. Topics Circuits Syst.*, vol. 4, no. 4, pp. 450–459, Dec. 2014.

[5] B. Ramakrishnan, I. K. Ngongiah, S. Çiçek, A. C. Chamgoué, and G. F. Kuiate, "Theoretical analysis of smooth nonlinear resistor–capacitor shunted Josephson junction circuit and its microcontroller-based digital design with graphic LCD," *Circuits, Syst., Signal Process.*, vol. 42, no. 1, pp. 47–62, Jan. 2023.

[6] X. Xu and M. Wiercigroch, "Approximate analytical solutions for oscillatory and rotational motion of a parametric pendulum," *Nonlinear Dyn.*, vol. 47, nos. 1–3, pp. 311–320, Dec. 2006.

[7] Y. Guo, Q. Wang, L. Yang, D. Zhang, X. Xue, and D. Yu, "A transient stability analysis method based on second-order nonuniform Kuramoto model," *Int. Trans. Electr. Energy Syst.*, vol. 30, no. 3, p. e1224, Mar. 2020.

[8] A. H. Salas and J. E. Castillo, "Exact solution to duffing equation and the pendulum equation," *Appl. Math. Sci.*, vol. 8, pp. 8781–8789, Jan. 2014.

[9] S. H. Strogatz, *Nonlinear Dynamics and Chaos With Student Solutions Manual: With Applications to Physics, Biology, Chemistry, and Engineering*. Boca Raton, FL, USA: CRC Press, 2018.

[10] Y. Makhlin, G. Scöhn, and A. Shnirman, "Josephson-junction qubits with controlled couplings," *Nature*, vol. 398, no. 6725, pp. 305–307, Mar. 1999.

[11] J. M. T. Thompson, H. B. Stewart, and R. Turner, "Nonlinear dynamics and chaos," *Comput. Phys.*, vol. 4, no. 5, pp. 562–563, 1990.

[12] S. Saha, A. A. Fouad, W. H. Kliemann, and V. Vittal, "Stability boundary approximation of a power system using the real normal form of vector fields," *IEEE Trans. Power Syst.*, vol. 12, no. 2, pp. 797–802, May 1997.

[13] C.-M. Lin, V. Vittal, W. Kliemann, and A. A. Fouad, "Investigation of modal interaction and its effects on control performance in stressed power systems using normal forms of vector fields," *IEEE Trans. Power Syst.*, vol. 11, no. 2, pp. 781–787, May 1996.

[14] J. Thapar, V. Vittal, W. Kliemann, and A. A. Fouad, "Application of the normal form of vector fields to predict interarea separation in power systems," *IEEE Trans. Power Syst.*, vol. 12, no. 2, pp. 844–850, May 1997.

[15] D. Cheng, J. Ma, Q. Lu, and S. Mei, "Quadratic form of stable sub-manifold for power systems," *Int. J. Robust Nonlinear Control, IFAC-Affiliated J.*, vol. 14, pp. 773–788, Jun. 2004.

[16] A. Xue, F. F. Wu, Y. Ni, S. Mei, and Q. Lu, "Power system transient stability assessment based on quadratic approximation of stability region," *Electric Power Syst. Res.*, vol. 76, nos. 9–10, pp. 709–715, Jun. 2006.

[17] A. C. Xue, K. L. Teo, Q. Lu, and S. W. Mei, "Polynomial approximations for the stable and unstable manifolds of the hyperbolic equilibrium point using semi-tensor product," *Int. J. Innov. Comput., Inf. Control*, vol. 2, no. 3, pp. 593–608, 2006.

[18] T. Kakutani and N. Sugimoto, "Krylov–Bogoliubov–Mitropolsky method for nonlinear wave modulation," *Phys. Fluids*, vol. 17, no. 8, pp. 1617–1625, Aug. 1974.

[19] H.-M. Liu, "Approximate period of nonlinear oscillators with discontinuities by modified Lindstedt–Poincare method," *Chaos, Solitons Fractals*, vol. 23, no. 2, pp. 577–579, Jan. 2005.

[20] A. H. Nayfeh, "Order reduction of retarded nonlinear systems—The method of multiple scales versus center-manifold reduction," *Nonlinear Dyn.*, vol. 51, no. 4, pp. 483–500, Mar. 2008.

[21] J. G. Yoder, "Chapter 3—Christiaan Huygens, book on the pendulum clock (1673)," in *Landmark Writings in Western Mathematics 1640–1940*. Amsterdam, The Netherlands: Elsevier, 2005, pp. 33–45.

[22] Q. Qiu, R. Ma, J. Kurths, and M. Zhan, "Swing equation in power systems: Approximate analytical solution and bifurcation curve estimate," *Chaos, Interdiscipl. J. Nonlinear Sci.*, vol. 30, no. 1, Jan. 2020, Art. no. 013110.

[23] F. Fontanela, A. Grolet, L. Salles, and N. Hoffmann, "Computation of quasi-periodic localised vibrations in nonlinear cyclic and symmetric structures using harmonic balance methods," *J. Sound Vibrat.*, vol. 438, pp. 54–65, Jan. 2019.

[24] W. Dai and J. Yang, "Vibration transmission and energy flow of impact oscillators with nonlinear motion constraints created by diamond-shaped linkage mechanism," *Int. J. Mech. Sci.*, vol. 194, Mar. 2021, Art. no. 106212.

[25] K. M. R. Shripad and S. Sundar, "Semi-analytical solution for a system with clearance nonlinearity and periodic excitation," *Nonlinear Dyn.*, vol. 111, no. 10, pp. 9215–9237, May 2023.

[26] S. L. Lau and Y. K. Cheung, "Amplitude incremental variational principle for nonlinear vibration of elastic systems," *J. Appl. Mech.*, vol. 48, no. 4, pp. 959–964, Dec. 1981.

[27] S. L. Lau and W.-S. Zhang, "Nonlinear vibrations of piecewise-linear systems by incremental harmonic balance method," *J. Appl. Mech.*, vol. 59, no. 1, pp. 153–160, Mar. 1992.

[28] Z. Yan, H. Dai, Q. Wang, and S. N. Atluri, "Harmonic balance methods: A review and recent developments," *Comput. Model. Eng. Sci.*, vol. 137, no. 2, pp. 1419–1459, 2023.

[29] B. Cochelin and C. Vergez, "A high order purely frequency-based harmonic balance formulation for continuation of periodic solutions," *J. Sound Vibrat.*, vol. 324, nos. 1–2, pp. 243–262, Jul. 2009.

[30] S. Karkar, B. Cochelin, and C. Vergez, "A high-order, purely frequency based harmonic balance formulation for continuation of periodic solutions: The case of non-polynomial nonlinearities," *J. Sound Vibrat.*, vol. 332, no. 4, pp. 968–977, Feb. 2013.

[31] H.-D. Chiang, F. F. Wu, and P. P. Varaiya, "A BCU method for direct analysis of power system transient stability," *IEEE Trans. Power Syst.*, vol. 9, no. 3, pp. 1194–1208, 1994.

[32] G. Wang, C. Wang, and M. Shahidehpour, "Neural network applications in hybrid data-model driven dynamic frequency trajectory prediction for weak-damping power systems," *IEEE Trans. Power Syst.*, early access, Aug. 14, 2023, doi: 10.1109/TPWRS.2023.3304791.

[33] H.-D. Chiang, *Direct Methods for Stability Analysis of Electric Power Systems: Theoretical Foundation, BCU Methodologies, and Applications*. Hoboken, NJ, USA: Wiley, 2011.

[34] P. S. Kundur and O. P. Malik, *Power System Stability and Control*, 2nd ed. New York, NY, USA: McGraw-Hill, 2022.

[35] V. Vittal, J. D. McCalley, and P. M. Anderson, *Power System Control and Stability*. Hoboken, NJ, USA: Wiley, 2019.

[36] A. A. Fouad and V. Vittal, *Power System Transient Stability Analysis Using the Transient Energy Function Method*. London, U.K.: Pearson, 1991.

JING LI received the B.Eng. and M.S. degrees from Northeast Electric Power University, Jilin, China, in 2017 and 2020, respectively. He is currently pursuing the Ph.D. degree with the College of Electrical Engineering, Zhejiang University, Hangzhou, China. His research interest includes power system stability analysis and control.

DEQIANG GAN (Senior Member, IEEE) received the Ph.D. degree in electrical engineering from Xi'an Jiaotong University, Xi'an, China, in 1994. From 1994 to 1998, he held research positions with Ibaraki University, the University of Central Florida, and Cornell University. From 1998 to 2002, he was with ISO New England Inc. Since 2002, he has been a Faculty Member with Zhejiang University, Hangzhou, China. From 2004 to 2006, he visited The University of Hong Kong. His research interest includes power system stability and control. From 2007 to 2014, he was an Editor of *European Transactions on Electrical Power*.

ZHENYAO LI received the B.Eng. degree from the School of Electrical and Electronic Engineering, Huazhong University of Science and Technology, Wuhan, China, in 2017, and the M.Eng. degree from the College of Electrical Engineering, Zhejiang University, Hangzhou, China, in 2021, where he is currently pursuing the Ph.D. degree. His research interest includes power system stability analysis and control.

HAO WU (Senior Member, IEEE) received the Ph.D. degree in electrical engineering from Zhejiang University, Hangzhou, Zhejiang, China. In 2002, he joined Zhejiang University. From 2003 to 2004, he visited The Hong Kong Polytechnic University. From 2009 to 2011, he also visited the University of Wisconsin–Madison. His current research interests include power system operation and stability, uncertainty analysis, cascading failure, load characteristic, and load modeling.

• • •